Proceedings of the 21st ICSMGE, Vienna, Austria, 14 – 19 June 2026. Pistrol, Adam & Schweiger (eds.)
Published by: ÖGG, Austrian Society for Geomechanics, Salzburg, Austria, ISBN 978-3-9503898-4-5
https://doi.org/10.53243/ICSMGE2026-1684

Cyclic triaxial test round-robin testing

N. Dufour, H. Calissano, L. Batilliot, T. Eon
GéoCoD/Cerema/Aix-en-Provence, France

L. Pigeot
Egis, Aix-en-Provence, France

I. Rogoff, C. Simon, A. Disantantonio
EDF-TEGG, Aix-en-Provence, France

T. Lando, E. Bourguignon
ANTEA Group, Orleans, France

ABSTRACT: In the context of seismic risk, a thorough understanding and characterization of soil behavior necessitates advanced geotechnical laboratory testing. Among these, cyclic triaxial tests play a critical role. The American standard ASTM D3999-11 outlines procedures for such tests, aimed at determining the shear modulus and damping characteristics of soils. The secant shear modulus and damping ratio derived from these tests are essential parameters for dynamic performance assessment of both natural and engineered structures subjected to cyclic or dynamic loading, such as that induced by earthquakes, ocean waves, or explosions. These parameters are commonly used in dynamic response analyses employing finite element methods, finite difference approaches, and both linear and nonlinear analytical models. In 2024, interlaboratory tests were initiated in France on two sandy materials: HN31 and a sandy mixture of HN38, HN34, HN31 and HN04. Three independent laboratories participated in this effort. The testing protocol involved the application of multiple successive sequences of undrained cyclic loading, covering a range of axial strains from 10^{-4} to 10^{-2}. The results from these cyclic triaxial tests are presented and discussed, focusing on the evolution of modulus vs strain. The influence of initial specimen conditions, such as reconstitution methods, saturation procedures, is also examined. Experimental results are compared with empirical models and those obtained from resonant column tests.

KEYWORDS: Cyclic triaxial test – round-robin test - sand

1 INTRODUCTION

Understanding the cyclic behavior of soils is critical for evaluating site response during earthquakes, as soil stiffness and damping directly influence ground motion amplification and potential structural damage. Under seismic loading, soils experience cyclic stress–strain paths that are nonlinear and hysteretic. At very small strains, stiffness is defined by the maximum shear modulus (G_{max}), related to shear wave velocity, typically measured *in situ* or through laboratory testing.

As shear strain increases, soil stiffness degrades and energy dissipation rises. In this range, behavior is described by the secant shear modulus (G), often normalized by Gmax for comparison. The damping ratio (D), representing energy loss per cycle, increases with strain. Both G and D depend on effective confining pressure, cyclic strain level, and soil structure.

Dynamic properties are assessed through field techniques and laboratory tests. Resonant column tests are suited for small strains ($\approx 10^{-6}$–10^{-4}), while cyclic triaxial tests, standardized by (ASTM, 2012), cover a broader range ($\approx 10^{-4}$–10^{-2}). These tests provide data for modulus reduction and damping curves essential for seismic response modeling.

Despite significant advances, accurate characterization of natural soils remains difficult due to sample disturbance and anisotropy. Interlaboratory variability in procedures and equipment calibration further complicates comparison. To address this, a round robin testing campaign was conducted involving multiple laboratories and standardized sandy materials. Tests were performed under consistent procedures, using both local and global strain measurement systems.

This study presents the results of the campaign, highlighting the influence of specimen preparation and measurement techniques on shear modulus estimation. The findings support improved reliability in dynamic soil property measurements and enhance confidence in numerical modeling used for seismic site response and engineering design.

2 EXPERIMENTAL PROGRAM

2.1 *Materials*

The materials used in this research consisted of two types of sand. The first was Hostun HN31 sand, whose properties have been extensively characterized in previous studies by various research laboratories (Baudouin, 2010). The second was a mixture of Hostun sands, composed of 25% (by dry weight) of the following fractions: HN38, HN34, HN32, and HN04 (with the HN04 fraction sieved at 0.63 mm).

Before testing, HN31 sand and the mixture were characterized by a coefficient of uniformity $C_u = D_{60}/D_{10}$ of 1.57 and 3.13, respectively, and a coefficient of curvature $C_c = {D_{30}}^2/D_{10}D_{60}$ of 1.03 and 0.96, respectively (Dufour et al., 2024).

2.2 *Preparation of specimens for testing*

Three procedures of reconstitution of the samples were used: compaction, raining and compaction followed by freezing. Only the density was fixed. Grain bulk density was measured: 26.00 kN/m^3.

5 HN31 specimens and 5 mixture specimens were reconstitued in laboratories (with a density objective of respectively, 19.22 and 20.21 kN/m^3). The height of the samples was about 100mm and the diameter about 50mm.

Void ratio of specimens before testing are presented in Figure 1 and Figure 2. Due to the use of different specimen reconstitution methods across laboratories, slight variations in

void ratio were observed. These differences may influence the initial state and mechanical response of the specimens, and are therefore taken into consideration in the interpretation of the test results.

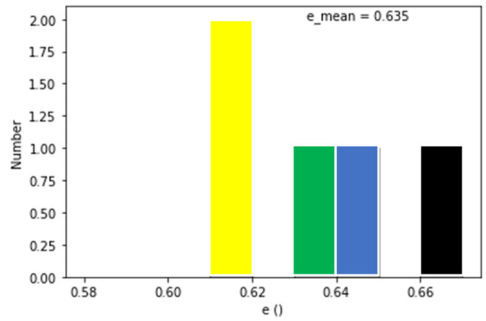

Figure 1. Void ratio distribution (HN31) before testing.

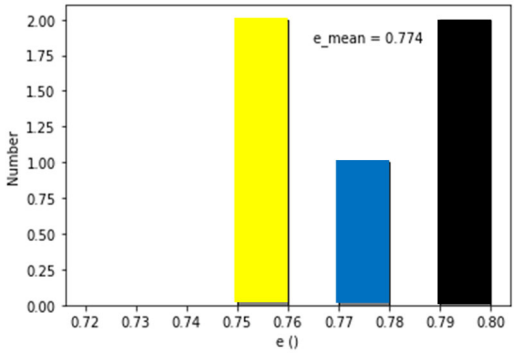

Figure 2. Void ratio distribution (mixture) before testing.

HN31 and mixture specimens presented respectively density between 18.96 and 19.30, and between 19.63 and 20.11 kN/m^3).

2.3 *Saturation and consolidation*

After reconstitution, the specimen was placed in the triaxial cell, which was equipped with an extension device. It is recommended to use a local strain measurement system attached directly to the specimen (Figure 3). Saturation of the soil was completed by applying back pressure increments. Finally, all specimens were saturated (Skempton coefficient 0,95<B<1,00). Then, they were consolidated at an isotropic pressure σ'_0 = 100 kPa (HN31) or 300 kPa (Mixture).

2.4 *Undrained cyclic loading*

Undrained cyclic loading was then applied, consisting of several successive sequences of displacement-controlled cycles. The imposed alternating sinusoidal axial displacement was defined by an amplitude and a frequency (here 0.5 Hz). This cyclic loading was kept constant until a predefined number of cycles was reached (here 50). The corresponding axial strain amplitude ε_a (double amplitude) (Serratrice, 2018) was recorded. From one sequence to the next, this amplitude is increased in order to cover a range of axial strains between 0.01% to 1%. If excessive pore pressure built up during a sequence (threshold determined by each laboratory), the specimen was re-consolidated under the isotropic effective confining pressure before initiating the next sequence. Throughout the cyclic shearing sequences, axial displacement both global and local measurements, axial force, and pore pressure were continuously recorded.

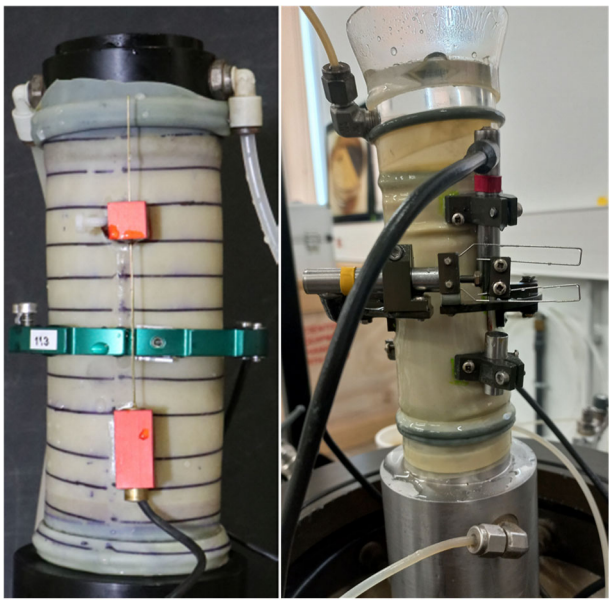

Figure 3. (Left) Hall-effect sensors (Antea group laboratory) and (Right) LVDT (EDF laboratory) sensors after testing.

For local strain measurements, two types of sensors were used: Hall-effect sensors (Figure 3, left) and LVDT sensors (Figure 3, right), both attached to the membrane in the central third of the specimen.

The deviatoric stress versus axial strain curves allow the measurement of the secant Young's modulus E for each cycle of each sequence. Assuming a Poisson's ratio $v = 0.5$, the shear modulus G is then derived as a function of shear strain γ (simple amplitude) (Equation 1).

$$G = \frac{E}{2(1+v)} \qquad \gamma = \frac{(1+v)\varepsilon_a}{2} \tag{1}$$

The G modulus measured at the smallest amplitudes and distortions is called G_{max}. It is derived n the following from the results of interlaboratory torsional resonant column tests conducted on the same material (Dufour et al., 2024).

3 RESULTS AND DISCUSSIONS

3.1 *Shear modulus as a function of shear strain*

Figures 4, 5, 6, and 7 show the variations of the shear modulus as a function of shear strain for: (i) HN31 sand based on global strain measurements, (ii) HN31 sand based on local strain measurements, (iii) the sand mixture based on global strain measurements, and (iv) the sand mixture based on local strain measurements, respectively.

Colors correspond to the initial void ratio of each specimen (from yellow to black presented in the histogram). The grey points represent the results obtained from previous torsional resonant column tests.

Symbols correspond to different specimen preparation: ● is linked with compaction followed by freezing, + to raining and ★ to compaction.

Two different apparatus were used (machine M1 ★ and machine M2 ● and +). Two different local strain measurement sensors were used (Hall-effect sensors ● and ★ and LVDT sensors +). The laboratories carried out several different tests on different specimens under the same drainage conditions and consolidation pressures.

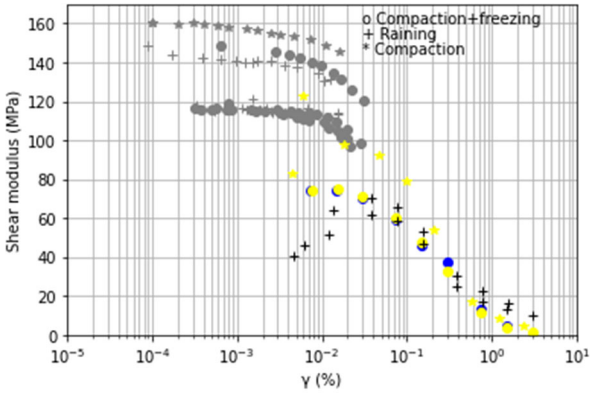

Figure 4. Shear modulus as function of distortion (HN31 - global strain measurements).

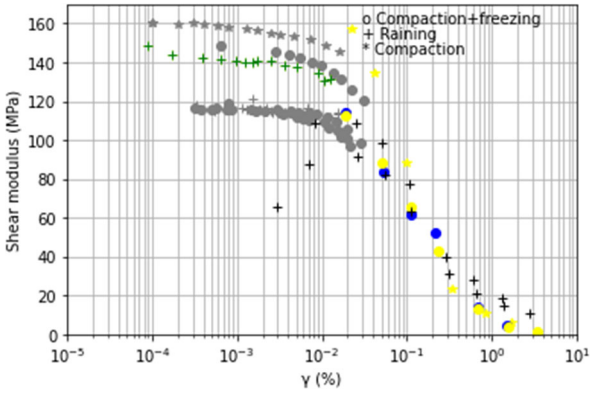

Figure 5. Shear modulus as function of distortion (HN31 - local strain measurements).

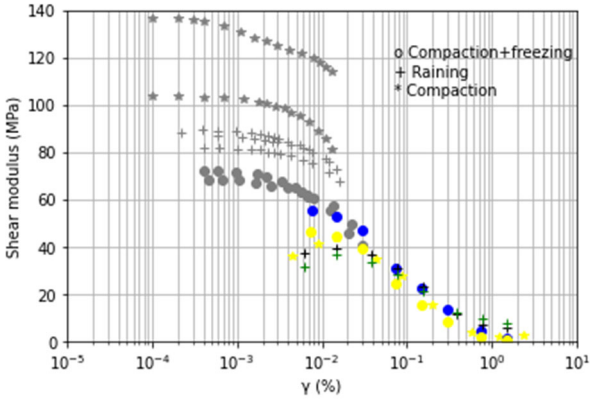

Figure 6. Shear modulus as function of distortion (mixture - global strain measurements).

A discrepancy is observed between the results obtained from local and global strain measurements. At low strain levels, global measurements tend to underestimate the corresponding moduli. It is also at these low strain levels that the largest differences between the results from the participating laboratories are observed, closely linked to the specific local measurement techniques employed. However, for shear strains greater than γ=10−2%, the results tend to converge regardless of the operator, the testing equipment, the specimen preparation method, or the initial void ratio.

More generally, repeatability of tests for the same laboratory is observed.

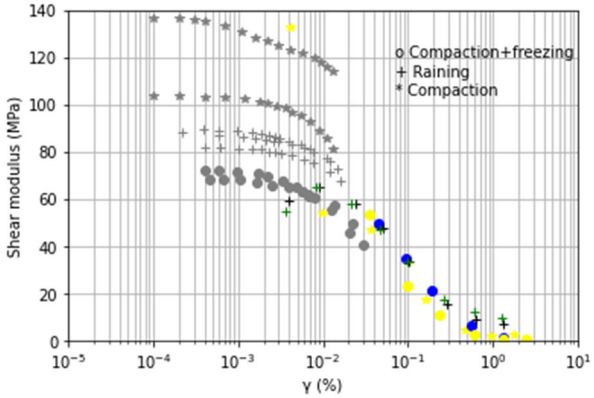

Figure 7. Shear modulus as function of distortion (mixture - local strain measurements).

3.2 *Discussion*

Experimental results were compared to empirical relationships (solid and dotted black lines) that have been proposed in the literature for sandy soils in Figures 8 and 9. Here only local strain measurements were taken into account. (Rollins et al., 2020) presented simplified equations for shear modulus degradation of sandy soils in relation with confining pressure and coefficient of uniformity (Equation 2 and 3) :

$$\frac{G}{G_{max}} = \frac{1}{1+\left(\frac{\gamma}{0.0063{\sigma_0'}^{0.38}}\right)^{0.87}} \quad (2)$$

$$\frac{G}{G_{max}} = \frac{1}{1+\left(\frac{\gamma}{0.0046{C_u}^{-0.197}{\sigma_0'}^{0.52}}\right)^{0.84}} \quad (3)$$

Normalized shear modulus is the current shear modulus G divided by G_{max}.

As shown in Figure 4 and 6, the values of G_{max} measured using the resonant column test varied between laboratories. To address this, the results from the cyclic triaxial tests conducted by each laboratory were normalized using the average G_{max} value reported by those same laboratories. Without this normalization approach, normalized modulus values exceeding 1 may appear, which are physically inconsistent and must be excluded. In extreme cases, this could result in the absence of valid modulus data in the strain range γ=10^{-2}% and 10^{-1}%, thereby undermining the value of using local displacement measurement systems.

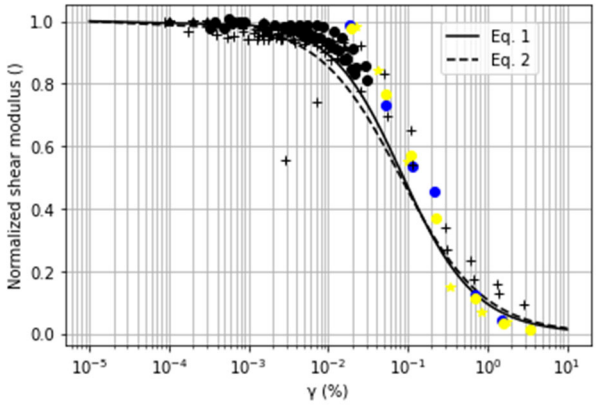

Figure 8. Normalized shear modulus as function of distortion (HN31 - local strain measurements).

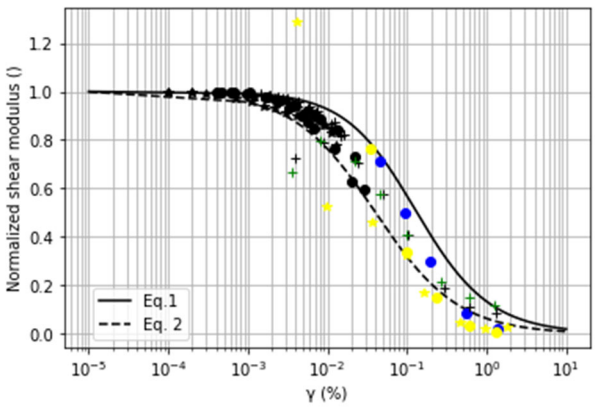

Figure 9. Normalized shear modulus as function of distortion (mixture - local strain measurements).

In Figure 8, the measured values of the shear modulus for HN31 specimens fluctuate around the empirical curves, whereas in Figure 9 (mixture), the empirical curves generally enclose the measured values and, in some cases, even lie above them, regardless of the model used.

These results can be explained with the grain size distribution curves obtained from a few specimens (randomly selected) after testing. Figures 10 and 11 present these results or HN31 sand and the mixture, respectively. The grain size distribution curves of HN31 sand after testing show little variation and are closely linked to the specimen preparation method, which is consistent with the results observed in Figure 8. In contrast, for the sand mixture, identical grain size distributions can lead to different shear modulus values.

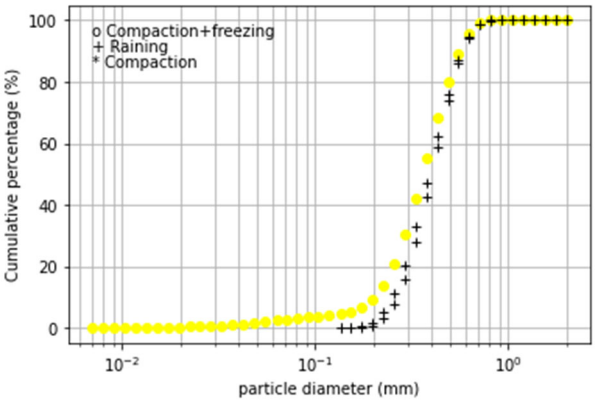

Figure 10. Particle-size size distribution (HN31) after testing.

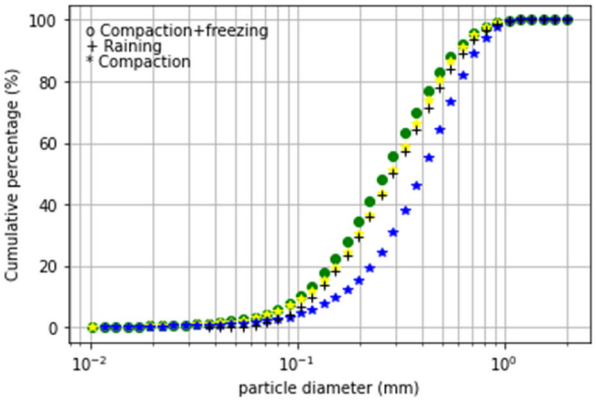

Figure 11. Particle-size size distribution (mixture) after testing.

4 CONCLUSIONS

An experimental program was conducted using two sandy materials: Hostun HN31 and a mixture of various Hostun fractions. Specimens were reconstituted using three preparation methods, targeting fixed densities. Due to varying methods, slight differences in void ratio were observed. Ten undrained cyclic triaxial tests were performed by three laboratories, applying sinusoidal loading at 0.5 Hz, with axial strains ranging from 0.01% to 1%. Local strain measurements were recorded using Hall-effect or LVDT sensors. Results show that global strain measurements tend to underestimate shear modulus at low strains. Despite variability in specimen preparation and instrumentation, normalized modulus reduction curves align well across laboratories and with empirical models. Differences in G_{max} values from resonant column tests required normalization to avoid inconsistent values. The findings support the use of local instrumentation and highlight interlaboratory repeatability. Future steps of the benchmark will focus on broadening and consolidating the experimental framework. First, the evolution of material damping with increasing strain levels will be systematically compared across laboratories. Additional tests will be performed on specimens composed of finer-grained matrials to assess the method's applicability to a wider range of soils. The number of participants will also be expanded by opening the benchmark to other European laboratories. In parallel, the testing procedure will be progressively refined and constrained, with the ultimate goal of establishing a common European protocol—and potentially a standardized method—for conducting cyclic triaxial tests.

5 ACKNOWLEDGEMENTS

The authors are grateful for the financial support provided by funding ANR (ANR-19-CE22-0015).

6 REFERENCES

ASTM. (2012). ASTM D3999-11 Standard Test Methods for the Determination of the Modulus and Damping Properties of Soils Using the Cyclic Triaxial Apparatus (ASTM D3999-11). https://doi.org/10.1520/D3999-11

Baudouin, G. (2010). *Sols renforcés par inclusions rigides : Modélisation physique en centrifugeuse de remblais et de dallage*. Université de Nantes.

Dufour, N., Calissano, H., Batilliot, L., Rogoff, I., Simon, C., Disantantonio, A., ... & Bourguignon, E. (2024). Resonant column round-robin testing. In *Geotechnical Engineering Challenges to Meet Current and Emerging Needs of Society* (pp. 1100-1103). CRC Press.

Rollins, K. M., Singh, M., & Roy, J. (2020). Simplified Equations for Shear-Modulus Degradation and Damping of Gravels. *Journal of Geotechnical and Geoenvironmental Engineering*, *146*(9), 04020076. https://doi.org/10.1061/(ASCE)GT.1943-5606.0002300

Serratrice, J.-F. (2018). Apport expérimental de la méthode de compactage statique des sols au laboratoire. Revue Française de Géotechnique, 156, Article 156. https://doi.org/10.1051/geotech/2019001